

Cycloidal Reluctance Magnetic Gears for High Gear Ratio Applications

Shima Hasanpour¹, *Student Member, IEEE*, Matthew Johnson², *Member, IEEE*,
Matthew C. Gardner³, *Member, IEEE*, and Hamid A. Toliyat¹, *Fellow, IEEE*

¹Department of Electrical and Computer Engineering, Texas A&M University, College Station, TX, USA

²U.S. Army Research Laboratory, U. S. Army DEVCOM, College Station, TX, USA

³Department of Electrical and Computer Engineering, University of Texas at Dallas, Richardson, TX, USA

At high gear ratios, surface permanent magnet (SPM) cycloidal magnetic gears (CyMGs) can achieve higher torque densities than SPM coaxial magnetic gears (CoMGs). This paper introduces the radial flux reluctance CyMG (Rel CyMG) topology and its operating principles. The Rel CyMG replaces the permanent magnets (PMs) on an SPM CyMG's inner rotor with salient teeth. Additionally, the Rel CyMG only requires half of the SPM CyMG's outer rotor PM count to achieve the same gear ratio, which simplifies assembly and allows the use of wider magnets. This may improve high gear ratio designs' manufacturability. A genetic algorithm was used with 2D finite element analysis to optimize Rel CyMGs, SPM CyMGs, and SPM CoMGs and demonstrate that SPM CyMGs significantly outperform the other topologies at higher gear ratios in terms of specific torque (ST) and PM ST. However, Rel CyMGs outperform SPM CoMGs at higher gear ratios, with respect to ST and PM ST. Rel CyMGs also eliminate the need for a PM retention sleeve and potentially enable the use of smaller air gaps, which can allow them to achieve slightly higher PM STs than SPM CyMGs at ultra-high gear ratios. Employing Halbach arrays significantly improves both CyMG topologies' ST.

Index Terms— Cycloidal magnetic gear, gear ratio, optimization, reluctance magnetic gear, torque, unbalanced magnetic forces.

I. INTRODUCTION

This paper introduces the radial flux reluctance cycloidal magnetic gear (Rel CyMG) topology, which is a modified version of a surface permanent magnet (SPM) cycloidal permanent magnet gear (CyMG) topology. The Rel CyMG is potentially more robust because it eliminates the permanent magnets (PMs) on the moving inner rotor. Additionally, the Rel CyMG requires half of the pole pair count on the outer rotor to achieve a given gear ratio, as compared to the SPM CyMG. This study compares the performances of the Rel CyMG, the SPM CyMG, and the SPM coaxial magnetic gear (SPM CoMG).

Magnetic gears have gained renewed attention because of the potential benefits of noncontact power transfer (in contrast to the mechanical contact between teeth in mechanical gears) for numerous applications such as wave energy [1], wind energy [2]-[3], traction [4], and aircraft [5]-[6]. A large portion of the literature on magnetic gears focuses on the SPM CoMG, which is shown in Fig. 1(a) [1]-[10]. An SPM CoMG contains three rotors: the inner low pole count, high-speed PM rotor (Rotor 1), the intermediate rotor consisting of ferromagnetic pieces (modulators) separated by nonmagnetic slots (Rotor 2), and the outer high pole count PM rotor (Rotor 3). Previous studies have shown that SPM CoMGs perform better at lower gear ratios [11]. High gear ratios require more PMs and modulators, which presents magnetic and manufacturing challenges, as discussed in [11].

Fig. 1(b) shows an SPM CyMG, which is the main alternative magnetic gear topology for high gear ratio applications [11]-[14]. This structure includes two rotors: the inner low pole count PM rotor (Rotor 1), and the outer high pole count PM rotor (Rotor 2). An SPM CyMG does not use modulators; therefore, it eliminates the highest piece count SPM CoMG rotor. In the most common implementation of an SPM CyMG, Rotor 2 is

held stationary, while the movement of Rotor 1 consists of two components, including a rotation around its own center, and an orbital revolution around the center of Rotor 2 [11]-[14]. Facilitating this complex motion pattern is the most significant structural challenge in the design of an SPM CyMG.

Operating at high gear ratios is electromagnetically and mechanically challenging for both SPM CoMGs and SPM CyMGs. In the most common configuration for both topologies, Rotor 1 accounts for the high-speed motion component. Holding the PMs on the surface of Rotor 1 can be mechanically challenging during high-speed rotation. Solutions have been proposed for this issue, such as using a sleeve around the PMs; however, this increases the effective air gap, which reduces the slip torque and may lead to eddy current losses [15]. Utilizing a consequent pole topology for Rotor 1 in CyMGs can potentially address the mechanical challenge of holding the PMs in place and eliminate the need for a PM retention sleeve, but the electromagnetic challenges of high gear ratio operation still remain [16]. Using an interior PM structure is another alternative; however, holding the magnets in place creates mechanical stress on the thin bridges. High gear ratios require high Rotor 1 PM pole counts for the SPM CyMG, which leads to undesirably thin bridges [17]. Also, the leakage paths through the thin bridges negatively affects the air gap flux.

Fig. 1(c) illustrates a Rel CyMG. In a Rel CyMG, the PMs on Rotor 1 of an SPM CyMG are replaced with teeth. This transformation is similar to the conversion of an SPM CoMG into a reluctance coaxial magnetic gear [18]-[19]. Rel CyMGs address the mechanical challenges of high-speed Rotor 1 operation in SPM CyMGs by replacing the Rotor 1 surface PMs with a reluctance structure. This gives Rel CyMGs a more mechanically robust rotor (as they have no moving magnets), which is potentially better suited for high-speed operation. However, as shown in [18], replacing PMs in a gear with a

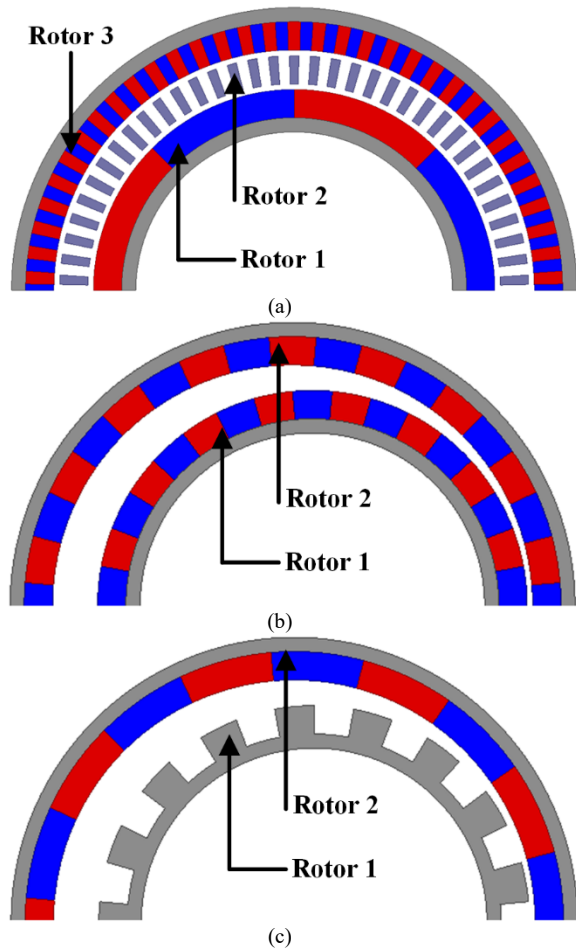


Fig. 1: Cross-sections of (a) an SPM CoMG, (b) an SPM CyMG, and (c) a Rel CyMG for gear ratios of 17.5:1, 17:1, and 17:1, respectively.

reluctance structure yields lower torque density designs due to the resulting decrease in flux density. This study introduces Rel CyMGs and their operating principles and compares the performances of optimal Rel CyMGs, SPM CyMGs, and SPM CoMGs across a range of gear ratios using a genetic algorithm (GA) and parametric 2D finite element analysis (FEA) simulations.

II. OPERATING PRINCIPLES

SPM CyMGs and SPM CoMGs have significant differences, but both topologies operate based on the same underlying principle. The magnetomotive force (MMF) associated with the PMs on a rotor is modulated by the air gap permeance function, which produces spatial harmonics similar to those associated with the other rotor's PMs. This enables the gearing behavior. Rotor 2 in an SPM CoMG consists of ferromagnetic modulators that create the permeance function required for the gearing effect. Optimal operation requires the number of modulators (Q_M) to be equal to the sum of the pole pairs on the inner rotor ($P_{1,SPMCoMG}$) and the pole pairs on the outer rotor ($P_{3,SPMCoMG}$), as given by (1). $P_{1,SPMCoMG}$ and $P_{3,SPMCoMG}$ must be chosen properly to avoid undesired torque ripples [2], [20]. The gear ratio depends on the operating mode, with the maximum gear

ratio achieved if Rotor 1 operates as the high-speed rotor and Rotor 2 operates as the low-speed rotor, while Rotor 3 is fixed. In this case, the gear ratio is given by (2), where ω_1 and ω_2 are the steady-state speeds of Rotor 1 and Rotor 2, respectively.

$$Q_M = P_{1,SPMCoMG} + P_{3,SPMCoMG} \quad (1)$$

$$G_{SPMCoMG}|_{\omega_3=0} = \frac{\omega_1}{\omega_2} = \frac{Q_M}{P_{1,SPMCoMG}} \quad (2)$$

An SPM CyMG has a time-varying, non-uniform air gap (due to the orbital motion of Rotor 1) that creates the permeance harmonics [11]-[13]. The optimal Rotor 2 pole pair count ($P_{2,SPMCyMG}$) is given by (3). The gear ratio for the stationary Rotor 2 configuration is given by (4), where ω_{Rot} is the speed of Rotor 1's rotation around its own axis and ω_{Orb} is the speed of the orbital revolution of Rotor 1 about the axis of Rotor 2, as explained in [12]-[13].

$$P_{2,SPMCyMG} = P_{1,SPMCyMG} + 1 \quad (3)$$

$$G_{SPMCyMG}|_{\omega_2=0} = \frac{\omega_{Orb}}{\omega_{Rot}} = -P_{1,SPMCyMG} \quad (4)$$

Rel CyMGs and SPM CyMGs have similar operating principles; however, a Rel CyMG's Rotor 1 teeth produce a permeance function instead of the MMF distribution produced by an SPM CyMG's Rotor 1 PMs. This is analogous to the replacement of an SPM CoMG's Rotor 1 PMs with teeth and slots to form a reluctance coaxial magnetic gear [18]. The Rotor 1 and air gap permeances, \mathcal{P}_1 and \mathcal{P}_{AG} , are given by (5) and (6), where N_1 is the number of teeth on Rotor 1. Equation (7) provides the Rotor 2 MMF produced by the PMs, \mathcal{F}_2 , based on the Rotor 2 pole pair count, $P_{2,RelCyMG}$. $\mathcal{P}_{1,0}$ and $\mathcal{P}_{AG,0}$ are the constant components of the Rotor 1 teeth and air gap permeance functions, and $\mathcal{P}_{1,i}$, $\mathcal{P}_{AG,j}$, and $\mathcal{F}_{2,k}$ represent the spatial harmonic coefficients for the Rotor 1 teeth permeance, air gap permeance, and Rotor 2 MMF functions. In these equations, ω_{Rot} and ω_{Orb} are the rotational and orbital speeds of Rotor 1, while ω_2 is the rotational speed of Rotor 2, and $\theta_{Rot,0}$, $\theta_{Orb,0}$, and $\theta_{2,0}$ represent the initial angular positions of Rotor 1 rotational motion, Rotor 1 orbital motion, and Rotor 2 rotational motion.

The MMF produced by a Rel CyMG's Rotor 2 PMs is modulated once by the permeance function of the air gap to produce the flux distribution given by $\Phi_{AG,2}$ in (8). $\Phi_{AG,2,0,k}$ is the set of flux spatial harmonics produced by the interaction of $\mathcal{P}_{AG,0}$ with $\mathcal{F}_{2,k}$, while $\Phi_{AG,2,j,k}$ is the set of flux spatial harmonics produced by the interaction of $\mathcal{P}_{AG,j}$ with $\mathcal{F}_{2,k}$, as defined in (9) and (10). Similarly, the Rotor 1 teeth permeance function modulates the Rotor 2 MMF to create the $\Phi_{1,2}$ flux distribution given by (11). $\Phi_{1,2,0,k}$ is the set of flux spatial harmonics produced by the interaction of $\mathcal{P}_{1,0}$ with $\mathcal{F}_{2,k}$, while $\Phi_{1,2,i,k}$ is the set of flux spatial harmonics produced by the interaction of $\mathcal{P}_{1,i}$ with $\mathcal{F}_{2,k}$, as defined in (12) and (13). The gearing action is achieved by selecting the tooth and PM pole pair counts to match the pole pair count and speed of one harmonic in (10)

$$\mathcal{P}_1(\theta) = \mathcal{P}_{1,0} + \sum_{i=1}^{\infty} \mathcal{P}_{1,i} \cos(iN_1(\theta - \omega_{Rot}t - \theta_{Rot,0})) \quad (5)$$

$$\mathcal{P}_{AG}(\theta) = \mathcal{P}_{AG,0} + \sum_{j=1}^{\infty} \mathcal{P}_{AG,j} \cos(j(\theta - \omega_{Orb}t - \theta_{Orb,0})) \quad (6)$$

$$\mathcal{F}_2(\theta) = \sum_{k=1}^{\infty} \mathcal{F}_{2,k} \cos(kP_{2,RelCyMG}(\theta - \omega_2t - \theta_{2,0})) \quad (7)$$

$$\Phi_{AG,2}(\theta) = \mathcal{F}_2(\theta)\mathcal{P}_{AG}(\theta) = \Phi_{AG,2,0,k}(\theta) + \Phi_{AG,2,j,k}(\theta) \quad (8)$$

$$\Phi_{AG,2,0,k}(\theta) = \sum_{k=1}^{\infty} \left\{ \mathcal{F}_{2,k} \mathcal{P}_{AG,0} \cos(kP_{2,RelCyMG}(\theta - \omega_2t - \theta_{2,0})) \right\} \quad (9)$$

$$\Phi_{AG,2,j,k}(\theta) = \sum_{j=1}^{\infty} \sum_{k=1}^{\infty} \left\{ \frac{\mathcal{F}_{2,k} \mathcal{P}_{AG,j}}{2} \cos\left((kP_{2,RelCyMG} \pm j) \left(\theta - \left(\frac{kP_{2,RelCyMG}\omega_2 \pm j\omega_{Orb}}{kP_{2,RelCyMG} \pm j} \right) t - \left(\frac{kP_{2,RelCyMG}\theta_{2,0} \pm j\theta_{Orb,0}}{kP_{2,RelCyMG} \pm j} \right) \right) \right) \right\} \quad (10)$$

$$\Phi_{1,2}(\theta) = \mathcal{F}_2(\theta)\mathcal{P}_1(\theta) = \Phi_{1,2,0,k}(\theta) + \Phi_{1,2,i,k}(\theta) \quad (11)$$

$$\Phi_{1,2,0,k}(\theta) = \sum_{k=1}^{\infty} \left\{ \mathcal{F}_{2,k} \mathcal{P}_{1,0} \cos(kP_{2,RelCyMG}(\theta - \omega_2t - \theta_{2,0})) \right\} \quad (12)$$

$$\Phi_{1,2,i,k}(\theta) = \sum_{i=1}^{\infty} \sum_{k=1}^{\infty} \left\{ \frac{\mathcal{F}_{2,k} \mathcal{P}_{1,i}}{2} \cos\left((kP_{2,RelCyMG} \pm iN_1) \left(\theta - \left(\frac{kP_{2,RelCyMG}\omega_2 \pm iN_1\omega_{Rot}}{kP_{2,RelCyMG} \pm iN_1} \right) t - \left(\frac{kP_{2,RelCyMG}\theta_{2,0} \pm iN_1\theta_{Rot,0}}{kP_{2,RelCyMG} \pm iN_1} \right) \right) \right) \right\} \quad (13)$$

with those of one harmonic in (13). This yields the relationship between N_1 and $P_{2,RelCyMG}$ given by (14), where k_a and k_b are odd integers, and i and j are integers and can be positive, 0, or negative. The relationship between the angular velocities of the motion components is given by (15). Selecting $k_a = 1$, $k_b = -1$, $j = -1$, and $i = 1$ yields (16) and (17). When Rotor 2 is stationary, the gear ratio is given by (18). The negative sign in (18) denotes that Rotor 1's rotation about its own axis is in the opposite direction of its orbital revolution around Rotor 2's axis. Fig. 2 demonstrates the operating principle of a Rel CyMG with $N_1 = 17$ and $P_{2,RelCyMG} = 9$, resulting in a gear ratio of 17:1. In order to illustrate this operating principle, two scenarios were evaluated: the scenario with the Rotor 1 teeth present but no axis offset and the scenario with an axis offset but no Rotor 1 teeth. Fig. 2(a) shows the air gap radial flux densities obtained for these two scenarios, and Fig. 2(b) shows the normalized FFTs of these air gap radial flux densities. Both scenarios produce a large 9th harmonic component corresponding to $P_{2,RelCyMG}$ and also an 8th harmonic component corresponding to

$$|k_a P_{2,RelCyMG} + j| = |k_b P_{2,RelCyMG} + iN_1| \quad (14)$$

$$\frac{k_a P_{2,RelCyMG}\omega_2 + j\omega_{Orb}}{k_a P_{2,RelCyMG} + j} = \frac{k_b P_{2,RelCyMG}\omega_2 + iN_1\omega_{Rot}}{k_b P_{2,RelCyMG} + iN_1} \quad (15)$$

$$2P_{2,RelCyMG} = N_1 + 1 \quad (16)$$

$$2P_{2,RelCyMG}\omega_2 = N_1\omega_{Rot} + \omega_{Orb} \quad (17)$$

$$G_{RelCyMG}|_{\omega_2=0} = \frac{\omega_{Orb}}{\omega_{Rot}} = -N_1 \quad (18)$$

$|P_{2,RelCyMG} - 1|$ or $|P_{2,RelCyMG} - N_1|$. In this case, it is the interaction of these 8th harmonic components that produces the gearing behavior. Figs. 3(a) and (b) illustrate the flux lines in these two scenarios.

High gear ratio designs contain high PM counts, which can

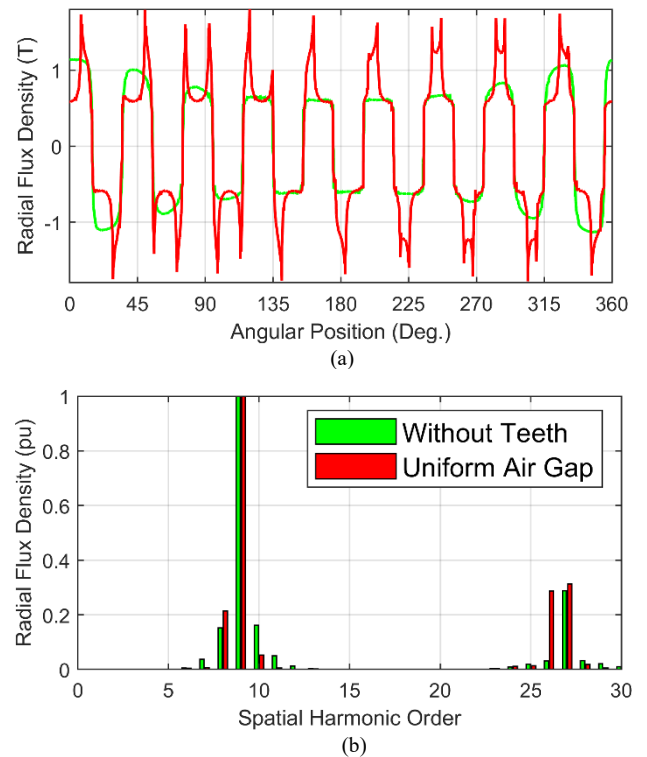


Fig. 2: (a) Distribution and (b) normalized FFT of the radial flux density for designs without teeth or with no axis offset (uniform air gap thickness).

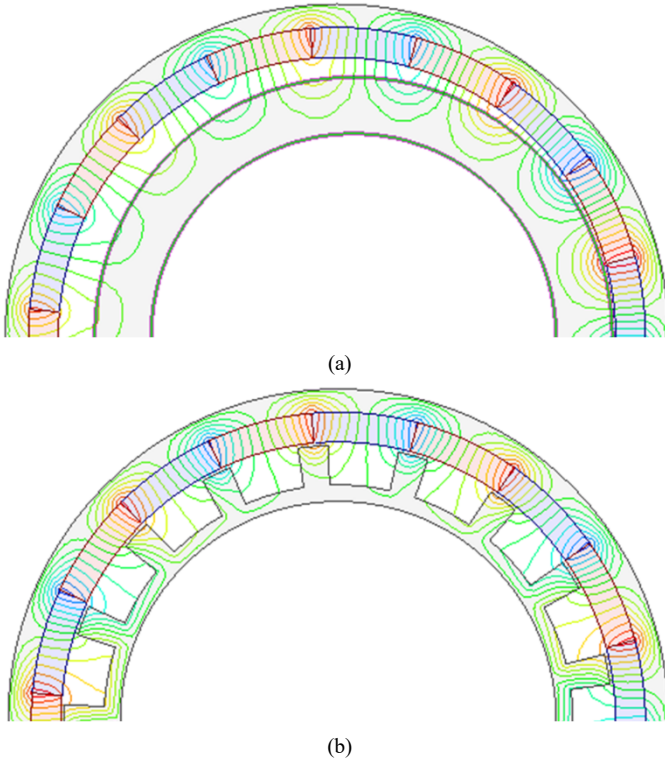


Fig. 3: Flux lines for (a) a design with a nonuniform air gap but no Rotor 1 teeth and (b) a design with a uniform air gap and Rotor 1 teeth.

complicate the manufacturing of a prototype. Comparing (3) and (4) with (16) and (18) reveals a potential advantage for Rel CyMGs. For a given gear ratio, $P_{2,RelCyMG}$ is half of $P_{2,SPMCyMG}$, which allows a Rel CyMG to use fewer and tangentially wider Rotor 2 PMs, as shown in Fig. 1.

III. DESIGN STUDY METHODOLOGY

A GA was used to independently optimize SPM CoMGs, SPM CyMGs, and Rel CyMGs for specific torque (ST), a design's slip torque divided by its active mass, and PM specific torque (PM ST), a design's slip torque divided by its PM mass, across gear ratios ranging from approximately 5:1 to 51:1, considering odd gear ratios to obtain feasible Rotor 2 pole pair counts in Rel CyMGs. In each optimization, the GA used 2D FEA to optimize a population of approximately 1000 designs over 100 generations with the objective of maximizing ST and PM ST across this range of gear ratios. The minimum air gap was fixed at 1 mm; however, the Rel CyMG designs were also optimized using a 0.75 mm minimum air gap because Rel CyMGs do not have any PMs on Rotor 1, so they do not require a PM retention sleeve on Rotor 1, which might enable the use of a smaller effective air gap. A broad range of values was considered for each design parameter, as listed in Table I. NdFeB N45UH was used for the PMs and Hiperc 50 was used for the back irons, modulators, and teeth.

The gear ratio in SPM CoMG topologies is defined as the ratio of the Rotor 1 speed to the Rotor 2 speed, with Rotor 3 fixed, as given by (2). The PM pole pair count on Rotor 1 of SPM CoMGs was varied in the range of 3 to 15. To avoid integer gear ratios, which result in designs with significant

TABLE I. GA PARAMETER VALUE RANGES

Parameter	Values
SPM CoMG integer part of the gear ratio (G_{Int})	5, 7, ... 51
Rel CyMG and SPM CyMG gear ratio (G)	5, 7, ... 51
Outer radius (R_{Out})	100 mm
Inner rotor back iron radial thickness ($T_{Bl,In,CyMG}$)	2 – 15 mm
SPM CyMG and SPM CoMG inner rotor PM radial thickness ($T_{PM,In}$)	3 – 20 mm
Rel CyMG inner rotor teeth radial thickness ($T_{TH,In}$)	3 – 20 mm
SPM CyMG and SPM CoMG inner rotor PM tangential fill factor ($\alpha_{PM,In}$)	0.1 – 1
Rel CyMG inner rotor teeth tangential fill factor ($\alpha_{TH,In}$)	0.3 – 0.5
Rel CyMG and SPM CyMG axis offset (T_{Off})	0.5 – 20 mm
SPM CoMG modulators radial thickness (T_{Mods})	3 – 20 mm
SPM CoMG modulators tangential fill factor ($\alpha_{Mods,In}$)	0.35 – 0.65
Outer rotor PM radial thickness ($T_{PM,Out}$)	3 – 20 mm
Outer rotor PM tangential fill factor ($\alpha_{PM,Out}$)	0.1 – 1
Outer back iron radial thickness ($T_{Bl,Out}$)	2 – 15 mm

torque ripple [2], [20]-[23], the PM pole pair counts on Rotor 3 were derived using (19). All the considered SPM CoMG designs have some symmetry, which cancels out unbalanced magnetic forces on the rotors [20], [23], since utilizing equations (1) and (19) ensures an even number of modulators for any design combination. CoMGs with only 1 or 2 pole pairs on Rotor 1 were not included because they cannot simultaneously achieve non-integer gear ratios and symmetry.

$$P_{3,SPMCoMG} = \begin{cases} (G_{Int} - 1)P_1 + 1 & \text{for } G_{Int}P_1 \text{ odd} \\ (G_{Int} - 1)P_1 + 2 & \text{for } G_{Int}P_1 \text{ even} \end{cases} \quad (19)$$

IV. RESULTS

Fig. 4 shows the results of the GA optimization studies. Table II summarizes the different design configurations whose performances are depicted in Figs. 4 and 5. Fig. 4 illustrates that a low gear ratio SPM CoMG can achieve higher ST and PM ST than a low gear ratio SPM CyMG or a low gear ratio Rel CyMG; however, as the gear ratio increases, the maximum achievable ST and PM ST decrease for the SPM CoMG and increase for the SPM CyMG and Rel CyMG. Generally, SPM CoMGs perform better at lower gear ratios because lower gear ratios result in more similar pole counts on both PM rotors, which enables better simultaneous optimization of both PM rotors [2], [18]. Torque is proportional to the derivative of co-energy with respect to mechanical angle. Increasing the number of pole pairs for a rotor increases the frequency of co-energy variation. However, increasing the number of poles will also reduce the amplitude of co-energy variation because there is more flux leaking between adjacent poles rather than crossing the air gap. Thus, there is an optimal pole pair count for each rotor, which balances these two competing considerations, where the torque is maximized. Because Rotor 1 and Rotor 3 have similar radii, they favor similar pole counts. As the gear ratio increases in SPM CoMGs, the ratio between P_1 and $P_{3,SPMCoMG}$ increases, which moves each of them farther from

their optimal values. P_1 decreases below its optimal value to minimize the extent to which $P_{3,SPMCoMG}$ increases beyond its optimum value. Thus, the performance of an SPM CoMG decreases as the gear ratio increases. The optimal SPM CoMG Rotor 1 pole count decreases to mitigate the extent to which the Rotor 3 pole count exceeds its optimal value as the gear ratio increases. This decreasing optimal Rotor 1 pole pair count (combined with the fact that pole pair count is a discrete value) results in the jagged portion of the optimal SPM CoMG Rotor 3 pole pair count curve in the low gear ratio region of Fig. 5(a). Once the optimal Rotor 1 pole pair count decreases to the minimum considered value, which is 3 in this study, the optimal Rotor 3 pole pair count increases linearly with gear ratio to extremely high and suboptimal values [20], as shown in Fig. 5(a).

Alternatively, in an SPM CyMG or a Rel CyMG, $P_{1,SPMCyMG}$ or N_1 is equivalent to the gear ratio, as indicated by (4) and (18), so these parameters cannot be optimized at a given gear ratio and increase linearly with gear ratio, as indicated in Fig. 5(a). Consequently, at a given radius and air gap, there is a nontrivial optimal $P_{1,SPMCyMG}$ or N_1 value (gear ratio) for SPM CyMGs and Rel CyMGs, respectively. As the gear ratio increases, the SPM CyMG quickly begins to achieve higher ST and PM ST than the SPM CoMG. Although the Rel CyMG never achieves a higher ST or PM ST than the SPM CyMG, it does eventually achieve

a higher ST and PM ST than the SPM CoMG at higher gear ratios. The optimal gear ratios for the SPM CyMG and the Rel CyMG and the gear ratios at which they begin to outperform the SPM CoMG depend on other design constraints such as the radius and the air gap. The Rel CyMG designs with 0.75 mm air gaps slightly outperform the Rel CyMG designs with 1 mm air gaps, but the smaller air gap does not help enough to overcome the decrease in ST and PM ST caused by removing the Rotor 1 PMs (in the conversion from an SPM CyMG to a Rel CyMG).

Fig. 5(a) and Fig. 5(b) show the corresponding outer rotor PM pole pair counts and PM arc lengths for the optimal designs in Fig. 4(a). Because $P_{1,SPMCoMG}$ was restricted to values of 3 or higher in order to eliminate torque ripple issues [20], the SPM CoMG designs have significantly higher outer rotor PM counts

TABLE II. LEGEND FOR DIFFERENT DESIGN CONFIGURATIONS CHARACTERIZED IN FIGS. 4 AND 5.

	Rel CyMG	SPM CyMG	SPM CoMG
Air gap (mm)	0.75	1	1

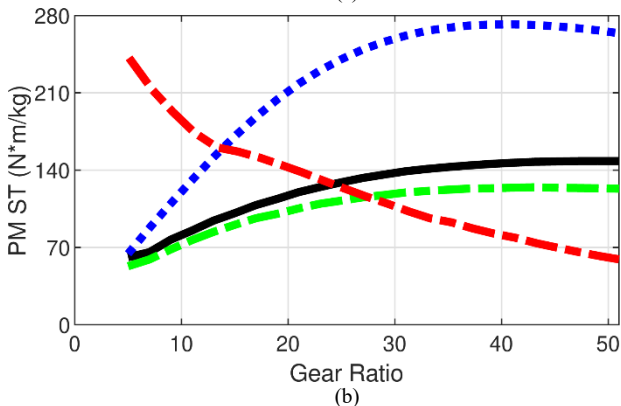
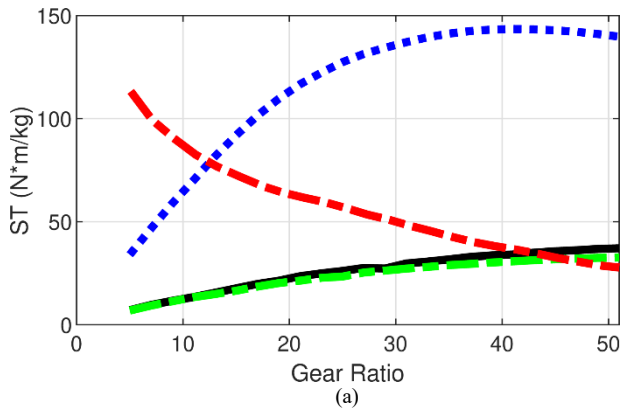


Fig. 4: Impact of gear ratio on the achievable (a) ST and (b) PM ST of SPM CoMGs, SPM CyMGs, and Rel CyMGs.

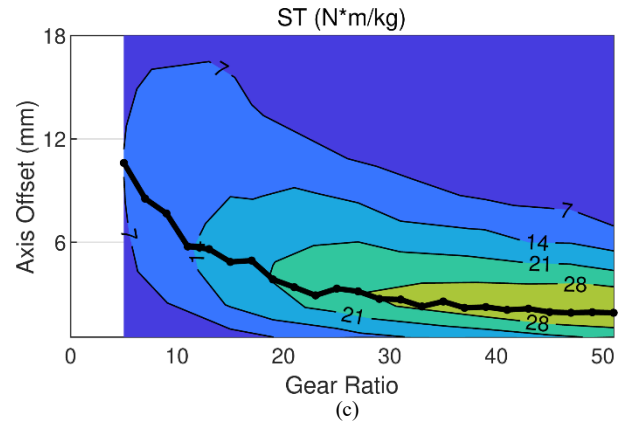
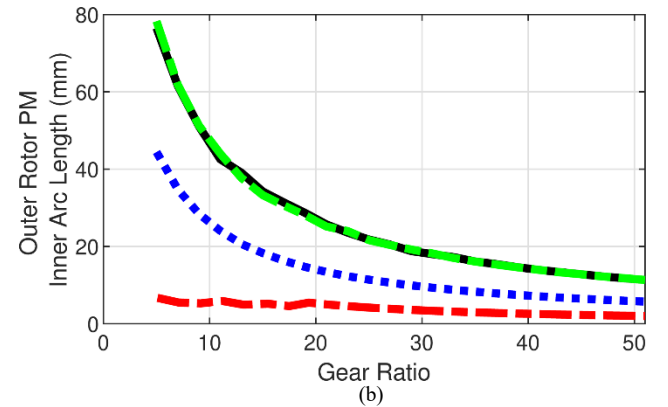
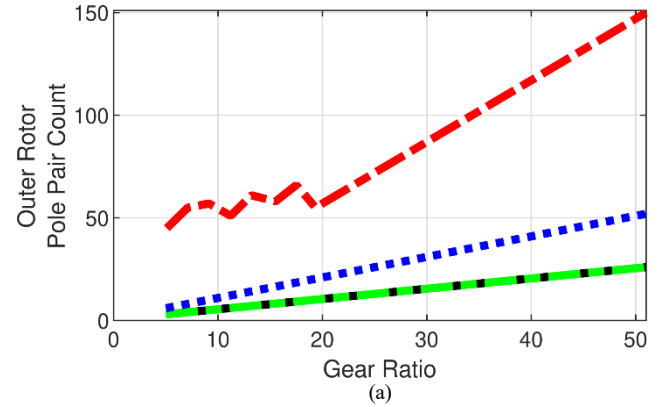


Fig. 5: Outer rotor PM (a) pole pair counts and (b) inner arc lengths for the maximum ST designs in Fig. 4(a). (c) Variation of maximum ST with gear ratio and axis offset for Rel CyMG designs with a 1 mm air gap. The black line indicates the optimal axis offset for each gear ratio.

than the cycloidal designs. As the gear ratio increases, all three topologies eventually experience a decrease in ST and PM ST once their outer rotor pole arcs become sub-optimally small and experience excessive leakage flux. Another challenge with extremely small PMs is that they are prone to breaking during assembly. Fig. 5(c) shows the optimal Rel CyMG axis offset between Rotors 1 and 2 corresponding to the maximum ST designs shown in Fig. 4(a). The pole pair counts increase with the gear ratio. Assuming a fixed outer radius, this means that the PMs have to be tangentially thinner. Consequently, the optimal axis offset decreases as the gear ratio increases, in part to create a smaller average effective air gap and counteract the increase in leakage flux per pole caused by smaller pole arcs.





As the gear ratio of an SPM CoMG increases, its ST and PM ST decrease dramatically, which is quite different than the design trends exhibited by the SPM CyMGs and Rel CyMGs. Therefore, the following studies only consider SPM CyMGs and Rel CyMGs with the parameter ranges mentioned in Table I. Additionally, Rel CyMGs with a 1 mm air gap were not considered for the comparisons below because the smaller 0.75 mm air gap enabled the Rel CyMGs to achieve slightly higher STs and PM STs.

Previous literature illustrated advantages of employing Halbach arrays in magnetic gears, such as increasing torque density [24]-[29] and efficiency [25], [29], [30], and reducing torque ripple [25]-[27]. Therefore, a GA was used to maximize the ST and PM ST of SPM CyMGs and Rel CyMGs utilizing a Halbach array with two pieces per pole over the same range of gear ratios and parameter values as presented in Table I. Also, since Halbach arrays may achieve higher torque densities without back irons [27], [30], air core (0 mm back iron thickness) designs were considered in addition to the back iron thicknesses in Table I. Table III summarizes the different scenarios characterized in Figs. 6-8.

Fig. 6 shows the maximum ST and PM ST values achieved for each different scenario across the range of considered gear ratios. Using Halbach arrays improves the achievable ST in both topologies, as shown in Fig. 6(a), since this PM arrangement favors air core designs to minimize the total active mass of a design. The flux path in a topology with a Halbach array and an air core passes through the tangentially magnetized PMs instead of the back iron. Therefore, the PMs tend to be thicker in designs with Halbach arrays to facilitate this flux path [27], which results in lower PM STs as shown in Fig. 6(b). However, as the gear ratio and, thus, the pole counts increase, the optimal designs require thinner back irons. Similarly, in designs with high gear ratios and Halbach arrays, thinner tangentially magnetized PMs are able to facilitate the flux paths. These thinner PMs are optimal for maximizing PM ST.

Fig. 7 illustrates the corresponding torque ripple percentage, the ratio of the peak-to-peak low-speed shaft torque ripple to the average low-speed shaft torque, for the maximum ST and PM ST designs shown in Fig. 6. Fig. 7(a) and 7(b) show that the torque ripple decreases at higher gear ratios for both topologies due to having more PMs involved in torque production. Also, at the higher gear ratios, the higher STs mean that a shorter stack length is required to provide the target

TABLE III. LEGEND FOR DIFFERENT DESIGN CONFIGURATIONS CHARACTERIZED IN FIGS. 6-8.

	Rel CyMG (0.75 mm air gap)	SPM CyMG (1 mm air gap)
Conventional PMs		
Halbach Array PMs		

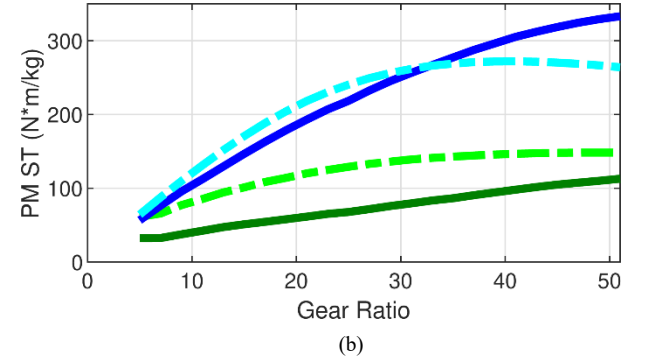
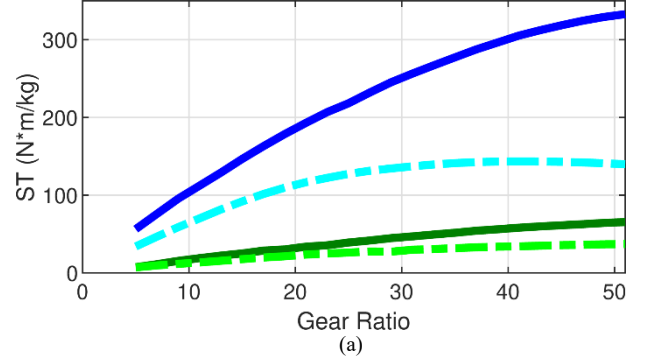


Fig. 6: Impact of gear ratio and Halbach arrays on the achievable (a) ST and (b) PM ST of SPM CyMGs and Rel CyMGs.

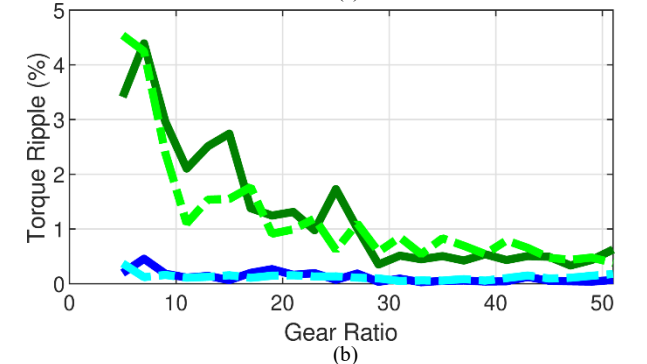
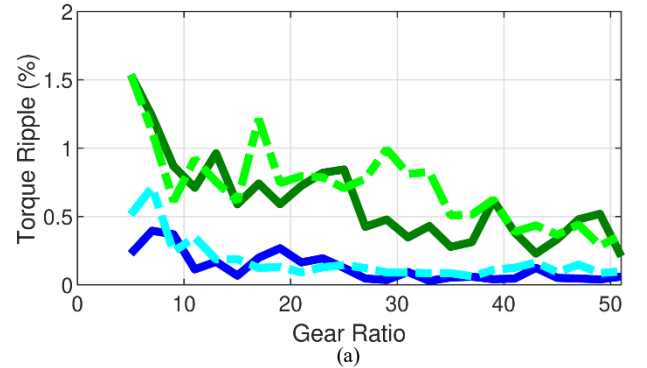


Fig. 7: Low-speed shaft torque ripple characteristic for maximum torque operation of SPM CyMGs and Rel CyMGs with maximum (a) ST and (b) PM ST.

torque, which reduces the peak-to-peak torque ripple present in the gear. The maximum PM ST designs exhibit higher torque ripples than the maximum ST designs, especially at lower gear ratios, due to the smaller effective air gap resulting from the thinner PMs in the maximum PM ST designs. These thinner effective air gaps do not filter out the higher order spatial harmonics of the air gap flux density as effectively as the thicker effective air gaps, and these higher order harmonics are what cause the torque ripple.

Fig. 8 shows the normalized torque and eccentric magnetic forces exerted on Rotor 1 as a function of the torque angle (the electromagnetic angle of Rotor 2 relative to the stable equilibrium zero-torque alignment) for the Rel CyMG and SPM CyMG designs with the highest STs and PM STs, based on the

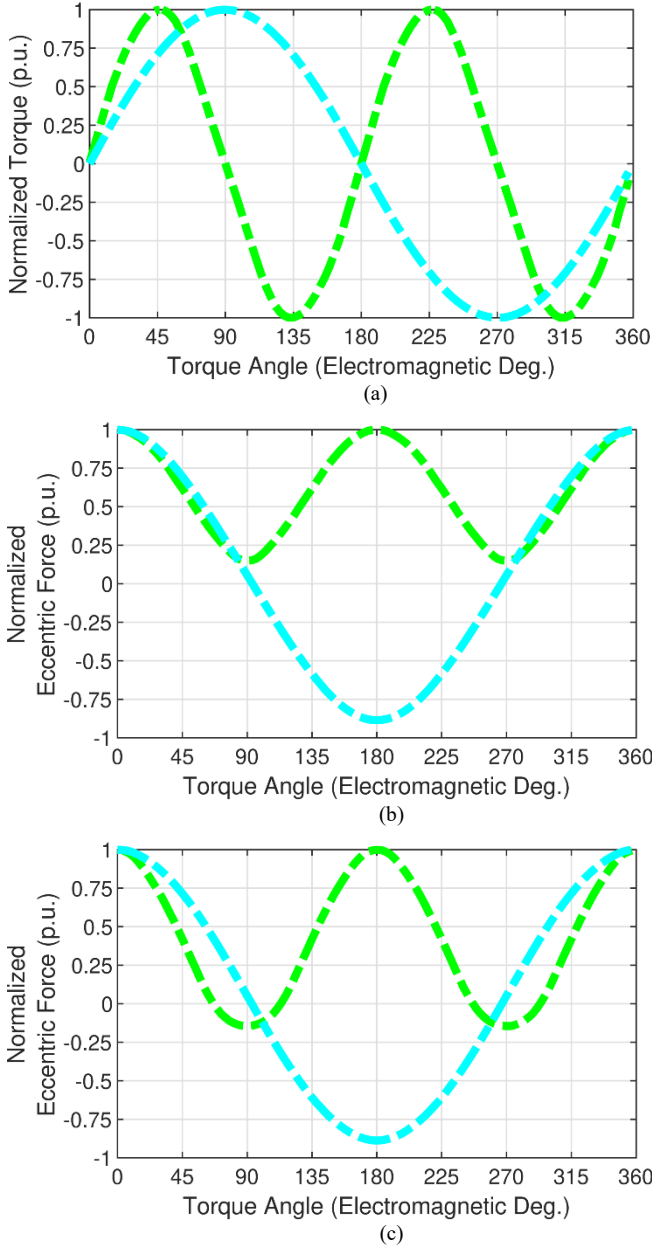


Fig. 8: (a) The normalized torque for the SPM CyMG and Rel CyMG designs with the maximum STs as a function of torque angle. The normalized magnetic eccentric force exerted on Rotor 1 as a function of torque angle for the SPM CyMG and Rel CyMG designs with the maximum (b) STs and (c) PM STs.

results shown in Fig. 6. The eccentric magnetic force on Rotor 1 is the force in the direction of the minimum air gap. For comparison purposes, each torque or force versus torque angle curve for a given design in Fig. 8 is normalized by its own maximum value and not by the overall maximum value in the graph. The eccentric forces in the Rel CyMG with maximum ST are positive values for any electromagnetic angle. Rel CyMGs eliminate PMs on Rotor 1; this eliminates any repulsive forces between Rotors 1 and 2. Therefore, Rel CyMGs can be designed to always experience positive magnetic forces in the direction of the minimum air gap as the ferromagnetic teeth are attracted to the PMs on Rotor 2. Also, the eccentric force and torque waveforms for Rel CyMGs in Fig. 8 peak twice in one electromagnetic cycle because the ferromagnetic teeth are attracted to the PMs regardless of the polarity of PMs. The non-zero eccentric force in the maximum PM ST Rel CyMG at its maximum torque angle (45 electromagnetic degrees) might be a potential advantage for Rel CyMGs, as it helps to balance the pin reaction forces, which are in the direction of the maximum air gap [31]. The net forces on Rotor 1 increase the bearing loads [14], [31]-[33]; therefore, reducing these forces can improve the reliability and efficiency of CyMGs, where friction losses in the bearings significantly reduce efficiency [31].

The trends in Fig. 4(b) indicate that the Rel CyMG might achieve higher PM STs than the SPM CyMG at significantly higher gear ratios. Therefore, higher gear ratios ranging between 101 and 301 were simulated with the same parameter value ranges in Table I, except the radial thicknesses for the various components were permitted to be as low as 1 mm to allow more flexibility in optimizing these designs, which have much shorter pole arcs. Fig. 9(a) shows the PM STs of the SPM and Rel CyMGs at these higher gear ratios. The optimal Rel

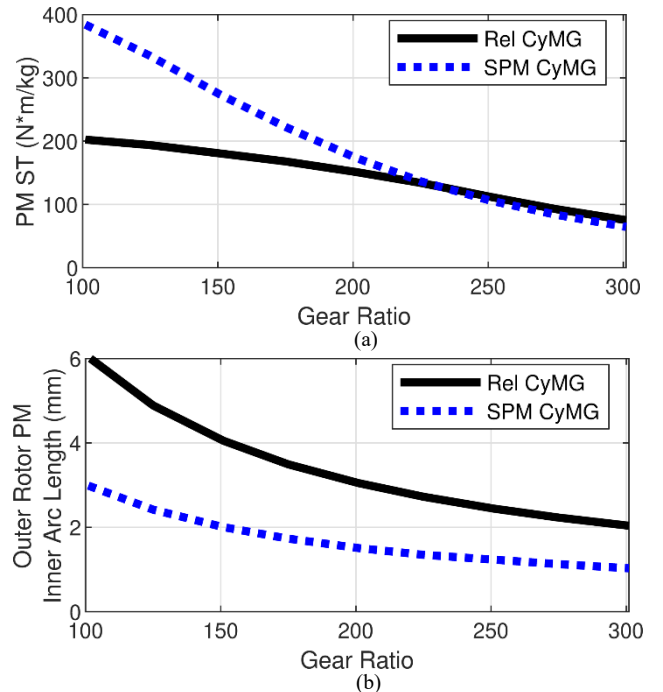


Fig. 9: (a) PM STs and (b) the corresponding outer rotor PM inner arc lengths of the optimal ultra-high gear ratio Rel CyMG and SPM CyMG designs (with gear ratios between 101 and 301).

CyMGs with gear ratios higher than 225 have slightly higher PM STs than the optimal SPM CyMGs. For a 301 gear ratio, the radial and tangential thicknesses of the PMs in the optimal SPM CyMGs are 1 mm, whereas, the tangential thickness of the PMs is 2 mm in the optimal Rel CyMGs, as shown in Fig. 9(b), which offers a potential manufacturing advantage for ultra-high gear ratio single-stage magnetic gears. However, both topologies achieve lower PM STs at these ultra-high gear ratios than they do at lower gear ratios.

V. SUMMARY OF RESULTS

The simulation results and analyses reveal the following conclusions.

- Optimal SPM CyMGs significantly outperform the other two topologies at higher gear ratios in terms of ST and PM ST. Thus, Rel CyMGs generally require more PM material than comparable SPM CyMGs.
- Rel CyMGs outperform SPM CoMGs at higher gear ratios.
- For a given gear ratio, Rel CyMGs require about one fourth as many PM poles as an SPM CyMG, which simplifies assembly.
- The PMs on the outer rotor of Rel CyMGs are tangentially wider than those in SPM CyMGs with the same gear ratio and radius, which can be an advantage in the manufacturing process, especially for high-gear ratio designs.
- Rel CyMGs may be more mechanically robust than SPM magnetic gears because all of the PMs are stationary.
- Halbach arrays reduce the overall active weight required to achieve a target torque for both SPM and Rel CyMGs.
- However, Halbach arrays reduce the PM ST for both SPM and Rel CyMG designs, except at very high gear ratios.
- The optimal SPM CyMGs experience less torque ripple than the optimal Rel CyMGs.
- A Rel CyMG can be designed to have positive eccentric forces over the full 360° electromagnetic angle with the reluctance rotor is always attracted to the outer rotor with PMs in the direction of the minimum air gap.
- The non-zero eccentric forces at the maximum torque angle in the Rel CyMG designs reflect a potential advantage to balance the pin reaction forces, which are a challenge in CyMG designs.
- The optimal Rel CyMGs can achieve slightly higher PM STs than the optimal SPM CyMGs at ultra-high gear ratios in a single stage. However, the PM STs of both topologies at these ultra-high gear ratios are much lower than at lower gear ratios.

VI. CONCLUSIONS

This paper introduces the reluctance (Rel) cycloidal magnetic gear (CyMG) topology and its operating principles. A GA was used to parametrically optimize surface permanent magnet (SPM) coaxial magnetic gears (CoMGs), SPM CyMGs, and Rel CyMGs for maximum specific torque (ST) and PM ST based on 2D FEA simulations over a broad range of parameter value ranges, as summarized in Table I.

Optimal Rel CyMGs use more PM material than optimal SPM CyMGs to achieve a given torque, within the considered range of gear ratios. Optimal Rel CyMGs use more PM material than optimal SPM CoMGs at lower gear ratios. Although Rel CyMGs achieve poor STs, they are more mechanically robust because they do not use any moving PMs and require half the outer rotor PM pole pair count, as compared to SPM CyMGs, to achieve a given gear ratio. This means that Rel CyMGs use tangentially wider PMs, which might be an advantage for assembling designs with high gear ratios. Additionally, at ultra-high gear ratios (>235:1), Rel CyMGs can achieve higher PM STs than SPM CyMGs. Thus, Rel CyMGs may be best suited for single-stage ultra-high gear ratio applications.

ACKNOWLEDGMENT

Portions of this research were conducted with the advanced computing resources provided by Texas A&M Performance Research Computing.

The authors would like to thank ANSYS for their support of the EMPE lab through the provision of FEA software.

REFERENCES

- [1] K. K. Uppalapati, J. Z. Bird, D. Jia, J. Garner, and A. Zhou, "Performance of a magnetic gear using ferrite magnets for low speed ocean power generation," in *Proc. IEEE Energy Convers. Congr. Expo.*, 2012, pp. 3348–3355.
- [2] N. Frank and H. Toliyat, "Gearing ratios of a magnetic gear for wind turbines," in *Proc. IEEE Int. Elect. Mach. Drives Conf.*, May 3–6, 2009, pp. 1224–1230.
- [3] K. Li *et al.*, "Electromagnetic analysis and experimental testing of a flux focusing wind turbine magnetic gearbox," *IEEE Trans. Energy Convers.*, vol. 34, no. 3, pp. 1512–1521, Sep. 2019.
- [4] T. Frandsen, L. Mathe, N. Berg, R. Holm, T. Matzen, P. Rasmussen, and K. Jensen, "Motor integrated permanent magnet gear in a battery electrical vehicle," *IEEE Trans. Ind. Appl.*, vol. 51, no. 2, pp. 1516–1525, Mar./Apr. 2015.
- [5] J. Scheidler, V. Asnani, and T. Talerico, "NASA's magnetic gearing research for electrified aircraft propulsion," in *Proc. AIAA/IEEE Elect. Aircraft Technol. Symp.*, 2018, pp. 1-12.
- [6] T. F. Talerico, Z. A. Cameron, J. J. Scheidler, and H. Hasseeb, "Outer stator magnetically-g geared motors for electrified urban air mobility vehicles," in *Proc. AIAA/IEEE Elect. Aircraft Technol. Symp.*, 2020, pp. 1-25.
- [7] K. Atallah and D. Howe, "A novel high-performance magnetic gear," *IEEE Trans. Magn.*, vol. 37, no. 4, pp. 2844–2846, Jul. 2001.
- [8] P. O. Rasmussen, T. O. Anderson, F. T. Jorgensen, and O. Nielsen, "Development of a high performance permanent magnetic gear," *IEEE Trans. Ind. Appl.*, vol. 41, no. 3, pp. 764-770, May/June 2005.
- [9] P. M. Tlali, R.-J. Wang, and S. Gerber, "Magnetic gear technologies: a review," in *Proc. IEEE Int. Conf. on Elect. Mach.*, 2014, pp. 544-550.
- [10] Y. Wang, M. Filippini, N. Bianchi, and P. Alotto, "A review on magnetic gears: topologies, computational models, and design aspects," *IEEE Trans. Ind. Appl.*, vol. 55, no. 5, pp. 4557-4566, Sep./Oct. 2019.
- [11] M. C. Gardner, M. Johnson and H. A. Toliyat, "Comparison of surface permanent magnet coaxial and cycloidal radial flux magnetic gears," in *Proc. IEEE Energy Convers. Congr. Expo.*, 2018, pp. 5005-5012.
- [12] J. Rens, K. Atallah, S. D. Calverley and D. Howe, "A novel magnetic harmonic gear," *IEEE Trans. Ind. Appl.*, vol. 46, no. 1, pp. 206-212, Jan./Feb. 2010.
- [13] F. T. Jorgensen, T. O. Andersen and P. O. Rasmussen, "The cycloid permanent magnetic gear," *IEEE Trans. Ind. Appl.*, vol. 44, no. 6, pp. 1659-1665, Nov./Dec. 2008.
- [14] K. Davey, T. Hutson, L. McDonald and G. Hutson, "The design and construction of cycloidal magnetic gears," in *Proc. IEEE Int. Elect. Mach. And Drives Conf.*, 2017, pp. 1-6.

- [15] L. Li, W. Li, D. Li, X. Zhang, and Y. Fan, "Influence of sleeve thickness and various structures on eddy current losses of rotor parts and temperature field in surface mounted permanent-magnet synchronous motor," *IET Elec. Power Appl.*, vol. 12, no. 8, pp. 1183-1191, 9 2018.
- [16] M. Johnson, S. Hasanpour, M. C. Gardner, and H. A. Toliyat, "Analysis and benchmarking of radial flux cycloidal magnetic gears with reduced permanent magnet piece count using consequent poles," in *Proc. IEEE Energy Convers. Congr. Expo.*, 2021, pp. 4334-4341.
- [17] F. Chai, Y. Li, P. Liang, and Y. Pei, "Calculation of the maximum mechanical stress on the rotor of interior permanent-magnet Synchronous motors," *IEEE Trans. Ind. Electron.*, vol. 63, no. 6, pp. 3420-3432, June 2016.
- [18] S. Hasanpour, M. C. Gardner, M. Johnson and H. A. Toliyat, "Comparison of reluctance and surface permanent magnet coaxial magnetic gears," in *Proc. IEEE Energy Convers. Congr. Expo.*, 2020, pp. 307-314.
- [19] K. Aiso, K. Akatsu, and Y. Aoyama, "A novel reluctance magnetic gear for high-speed motor," *IEEE Trans. Ind. Appl.*, vol. 55, no. 3, pp. 2690-2699, May-June 2019.
- [20] B. Praslicka, M. C. Gardner, M. Johnson and H. A. Toliyat, "Review and analysis of coaxial magnetic gear pole pair count selection effects," *IEEE J. Emerg. Sel. Topics Power Electron.*, early access. doi: 10.1109/JESTPE.2021.3053544.
- [21] M. Johnson, M. C. Gardner, and H. A. Toliyat, "Design comparison of NdFeB and ferrite radial flux surface permanent magnet coaxial magnetic gears," *IEEE Trans. Ind. Appl.*, vol. 54, no. 2, pp. 1254-1263, Mar./Apr. 2018.
- [22] M. Johnson, M. C. Gardner, H. A. Toliyat, S. Englebretson, W. Ouyang, and C. Tschida, "Design, construction, and analysis of a large-scale inner stator radial flux magnetically geared generator for wave energy conversion," *IEEE Trans. Ind. Appl.*, vol. 54, no. 4, pp. 3305-3314, Jul./Aug. 2018.
- [23] G. Jungmayr, J. Loeffler, B. Winter, F. Jeske, and W. Amrhein, "Magnetic gear: radial force, cogging torque, skewing, and optimization," *IEEE Trans. Ind. Appl.*, vol. 52, no. 5, pp. 3822-3830, Sep./Oct. 2016.
- [24] L. Jian and K. T. Chau, "A coaxial magnetic gear with Halbach permanent-magnet arrays," *IEEE Trans. Energy Convers.*, vol. 25, no. 2, pp. 319-328, Jun. 2010.
- [25] L. Jian, K. T. Chau, Y. Gong, J. Z. Jiang, C. Yu and W. Li, "Comparison of coaxial magnetic gears with different topologies," *IEEE Trans. Magn.*, vol. 45, no. 10, pp. 4526-4529, Oct. 2009.
- [26] A. Rahideh, A. A. Vahaj, M. Mardaneh, and T. Lubin, "Two-dimensional analytical investigation of the parameters and the effects of magnetisation patterns on the performance of coaxial magnetic gears," *IET Elec. Syst. Transp.*, vol. 7, no. 3, pp. 230-245, Aug. 2017.
- [27] M. Johnson, M. C. Gardner, and H. A. Toliyat, "Analysis of axial field magnetic gears with Halbach arrays," in *Proc. IEEE Int. Elect. Mach. and Drives Conf.*, 2015, pp. 108-114.
- [28] H. Huang, R. Qu and J. Bird, "Performance of Halbach cycloidal magnetic gears with respect to torque density and gear ratio," in *Proc. IEEE Int. Elect. Mach. and Drives Conf.*, 2019, pp. 1977-1984.
- [29] T. F. Talerico, J. J. Scheidler, and Z. A. Cameron, "Electromagnetic mass and efficiency of magnetic gears for electrified aircraft," in *Proc. AIAA/IEEE Elect. Aircraft Technol. Symp.*, 2019, pp. 1-25.
- [30] M. C. Gardner, M. Johnson, and H. A. Toliyat, "Performance impacts of practical fabrication tradeoffs for a radial flux coaxial magnetic gear with Halbach arrays and air cores," in *Proc. IEEE Energy Convers. Congr. Expo.*, 2019, pp. 3129-3136.
- [31] B. Praslicka *et al.*, "Practical analysis and design of a 50:1 cycloidal magnetic gear with balanced off-axis moments and a high specific torque for lunar robots," in *Proc. IEEE Int. Elect. Mach. Drives Conf.*, 2021, pp. 1-8.
- [32] H. Huang, J. Z. Bird, A. L. Vera, and R. Qu, "An axial cycloidal magnetic gear that minimizes the unbalanced radial force," *IEEE Trans. Magn.*, vol. 56, no. 7, pp. 1-10, Jul. 2020.
- [33] K. Davey, L. McDonald, and T. Hutson, "Axial flux cycloidal magnetic gears," *IEEE Trans. Magn.*, vol. 50, no. 4, pp. 1-7, Apr. 2014.

BIOGRAPHIES



Shima Hasanpour (S' 18) earned her B.S. in electrical engineering from Sharif University of Technology, Tehran, Iran in 2018. She is currently pursuing a Ph.D. in electrical engineering while working in the Advanced Electric Machines and Power Electronics Laboratory at Texas A&M University. Her research interests include the optimal design and control of electric machines, magnetic gears, and magnetically geared machines.



Matthew Johnson (S' 13, M'17) earned his B.S. and Ph.D. both in electrical engineering from Texas A&M University, College Station, Texas, in 2011 and 2017, respectively. He is currently an electronics engineer for the U.S. Army Research Laboratory. His research interests include the design and control of electric machines and magnetic gears.



Matthew C. Gardner (S' 15, M' 19) earned his B.S. in electrical engineering from Baylor University, Waco, Texas in 2014. He earned his Ph.D. in electrical engineering from Texas A&M University, College Station, Texas in 2019. In 2020, he joined the University of Texas at Dallas, Richardson, Texas as an assistant professor of electrical and computer engineering. His research interests include optimal design and control of electric machines and magnetic gears.



Hamid A. Toliyat (S'87, M'91, SM'96, F'08) received the B.S. degree from Sharif University of Technology, Tehran, Iran in 1982, the M.S. degree from West Virginia University, Morgantown, WV in 1986, and the Ph.D. degree from University of Wisconsin-Madison, Madison, WI in 1991, all in electrical engineering. In March 1994 he joined the Department of Electrical and Computer Engineering, Texas A&M University where he is currently the Raytheon endowed professor of electrical engineering. Dr. Toliyat has many papers and awards to his name, including the Nikola Tesla Field Award.